PAPER • OPEN ACCESS

Raman superradiance and spin lattice of ultracold atoms in optical cavities

New Journal of Physics
The open access journal for physics

Raman superradiance and spin lattice of ultracold atoms in optical cavities

S Safaei[1,3], Ö E Müstecaplıoğlu[2] and B Tanatar[1]

[1] Department of Physics, Bilkent University, Bilkent, 06800 Ankara, Turkey
[2] Department of Physics, Koç University, Sarıyer, 34450 Istanbul, Turkey
E-mail: safaei@fen.bilkent.edu.tr

New Journal of Physics **15** (2013) 083037 (14pp)
Received 1 April 2013
Published 20 August 2013
Online at http://www.njp.org/
doi:10.1088/1367-2630/15/8/083037

Abstract. We investigate the synthesis of a hyperfine spin lattice in an atomic Bose–Einstein condensate, with two hyperfine spin components, inside a one-dimensional high-finesse optical cavity, using off-resonant superradiant Raman scattering. Spatio-temporal evolution of the relative population of the hyperfine spin modes is examined numerically by solving the coupled cavity–condensate mean-field equations in the dispersive regime. We find, analytically and numerically, that beyond a certain threshold of the transverse laser pump, Raman superradiance and self-organization of the hyperfine spin components occur simultaneously and as a result a magnetic lattice is formed. The effects of an extra laser pump parallel to the cavity axis and the time dependence of the pump strength on the synthesis of a sharper lattice are also addressed.

[3] Author to whom any correspondence should be addressed.

Contents

1. Introduction

An atomic gas inside a high-finesse optical cavity [1, 2] may exhibit self-organization when it is subjected to a transverse laser pump [3–7]. In matter–cavity quantum electrodynamic (QED) systems, the mechanical effect of the electromagnetic fields on the motional states of atoms and the phase shift effect of atomic motion on the fields induce each other mutually in a self-consistent loop. The idea of trapping atomic Bose–Einstein condensates (BECs) in high-finesse optical cavities [8] has been experimentally realized and developed [9–12] to allow for sufficiently strong cavity–condensate coupling in order to realize nonlinear effects, such as bistability, even with the cavity photon number below unity [13–16] and to probe quantum phases of the condensate by cavity photons [17]. Quite recently, the Dicke superradiance quantum phase transition [18–20] in a BEC–cavity system [21] has been demonstrated [22, 23] and the nonequilibrium dynamics of such systems have been studied [24, 25] taking into account the finite size effects [26, 27] and examining the nonequilibrium effects at the critical point [27, 28].

The Dicke quantum phase transition for the single-mode BEC inside a high-finesse cavity [22] is characterized by an abrupt increase in the number of cavity photons, after a certain threshold of the pump intensity, which is accompanied by broken translational symmetry of the condensate with the formation of an optical lattice [29]. Pump–cavity photon scattering couples the initial zero-momentum state of BEC to a superposition of higher recoil momentum states [24]. A quite different scenario happens if a condensate of atoms with two different hyperfine states is pumped by a laser field far detuned from the atomic transition [30, 31]; that is, Raman superradiance [32, 33] may occur during which the hyperfine state of atoms changes.

There has been much interest in multi-mode atom–cavity systems recently, such as bosonic Josephson junctions inside a single-mode cavity [34] and spin glasses of single-component BEC in a multi-mode cavity [35]. Optical bistability has been studied in spin-1 [36, 37] and in two-mode BECs [16, 38]. Multi-species systems provide a very rich platform for the investigation of phase transitions, in addition to their practical advantages such as faster self-organization with lower threshold [39], and efficient, easily interpretable imaging of correlations in phase transitions by the cavity field [27, 40].

In this paper, we examine the idea of the Dicke-like phase transition in a system of a BEC–cavity with Raman coupling as well as the formation of magnetic lattices in the condensate. We consider a two-mode BEC, where the two modes correspond to two

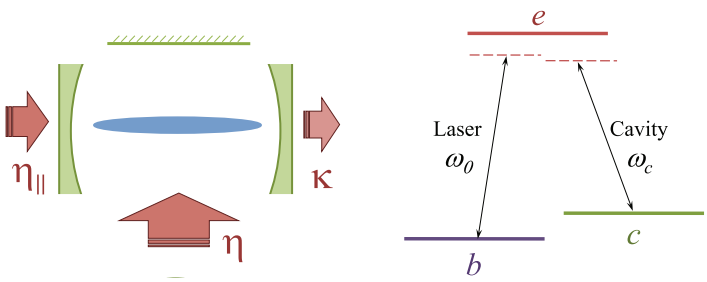

Figure 1. Left: schematic drawing of a BEC in a one-dimensional optical cavity subject to parallel and transverse laser fields. The cavity has a decay rate of κ. Right: the doublet of lower levels (b and c) of the BEC atoms is coupled by a cavity field and a laser field via the atomic excited state e in Raman scattering scheme. Both the laser field and the cavity field are far detuned from the atomic transition frequencies.

hyperfine states of the atoms, inside a one-dimensional optical cavity pumped by a laser field perpendicular to the cavity axis. The two modes of the condensate are coupled in a Raman scheme through a cavity mode and a laser field. The laser field and the cavity mode are far detuned from the atomic transition and therefore the system is in the dispersive regime. Moreover, the laser field is slightly detuned from the cavity resonance. Numerically solving the coupled nonlinear dynamical equations of the system, we show that beyond a certain value of the transverse pump strength, atoms scatter the laser field into the cavity mode and, in return, themselves move to the higher hyperfine state. As a result, Raman superradiance and translational symmetry breaking of the condensate take place simultaneously. The latter, which is a result of self-organization of atoms in the higher hyperfine state, leads to the formation of a ferromagnetic or ferrimagnetic lattice, depending on the rate of Raman transition. In this work, we have also addressed the effect of an extra parallel pump and the time dependence of the transverse pump on the synthesis of a well-defined magnetic lattice.

The rest of this paper is organized as follows. In section 2, we introduce our BEC–cavity model and derive the mean-field equations that govern the dynamics of the cavity–matter system. In section 3.1, we calculate the critical value of transverse pump strength after which Raman superradiance takes place using the first-order perturbation approach. The results of the numerical solution of the dynamical equations are presented in section 3.2. In section 4, we discuss and address the effect of an extra parallel pump and a time-dependent pump for practical synthesis of a sharp and stable magnetic lattice. We summarize our results in section 5.

2. Model

We consider a condensate of N atoms with two non-degenerate hyperfine states, $|b\rangle$ and $|c\rangle$, in a one-dimensional single-mode cavity of frequency ω_c as shown in figure 1. With an appropriate design of a trap, one can isolate two desired hyperfine states ($|m_F = -1\rangle$ and $|m_F = 1\rangle$) from the rest. In such a case, since other hyperfine states will be expelled from the trap, any inelastic atomic collision resulting in transition of atoms to other hyperfine states would lead to particle loss from the trap. At low temperatures, the rate of particle loss is very small in cold atomic gases and specifically in the condensates [41–43]. We, thus, omit particle loss in the present

calculations. The hyperfine states are coupled to an excited state $|e\rangle$ (with $m_F = 0$) by a transverse pump of frequency ω_0 and the cavity field in the Raman scheme where coupling of each field to the other transition as well as coupling of the other cavity mode with the same frequency but opposite polarization are forbidden due to conservation of angular momentum (a system in which both polarizations of the cavity field are coupled to several hyperfine states is studied in [44]). The cavity is driven by another laser with the same frequency ω_0. In the dispersive regime where the fields are far detuned from the atomic transitions, the Hamiltonian of the system [32, 33] can be written as

$$H = \sum_{j=b,c} \int \mathrm{d}x\ \psi_j^\dagger \left(-\frac{\hbar^2}{2m}\frac{\partial^2}{\partial x^2} + V_j(x) + \hbar\omega_{bc}\delta_{j,c} \right) \psi_j + H_{\mathrm{Raman}} + \sum_{i,j=b,c} \int \mathrm{d}x\ \frac{u_{ij}}{2}\psi_i^\dagger \psi_j^\dagger \psi_j \psi_i + \hbar\omega_c a^\dagger a - \mathrm{i}\hbar\eta_{||}(a\mathrm{e}^{\mathrm{i}\omega_0 t} - a^\dagger \mathrm{e}^{-\mathrm{i}\omega_0 t}), \quad (1)$$

where $\psi_j(x,t)$ ($\psi_j^\dagger(x,t)$) is the annihilation (creation) operator for a bosonic atom at the space–time point (x,t). $V_j(x)$ is the external trap potential for the state $j = b, c$ and ω_{bc} is the frequency of the $b \leftrightarrow c$ transition. $\{u_{ij}\}$ are the interaction strengths of atoms in states i and j and are related to s-wave scattering lengths $\{a_{ij}\}$ through $u_{ij} = 4\pi\hbar^2 a_{ij}/(mw^2)$, where m is the mass of atoms and w is the transverse size of the condensate. The parallel laser field strength is denoted by $\eta_{||}$ and the annihilation (creation) operator of the cavity mode is a ($a^\dagger$). For a cavity mode with wave number k, the Raman scattering Hamiltonian (H_{Raman}) has the form

$$H_{\mathrm{Raman}} = -\mathrm{i}\hbar \int \mathrm{d}x\ \psi_e^\dagger h_0(\mathrm{e}^{-\mathrm{i}\omega_0 t} + \mathrm{e}^{\mathrm{i}\omega_0 t})\psi_b + \mathrm{h.c.} - \mathrm{i}\hbar \int \mathrm{d}x\ \psi_e^\dagger g_0 \cos(kx)(a + a^\dagger)\psi_c + \mathrm{h.c.}, \quad (2)$$

where h_0 and g_0 are the atom–pump and atom–cavity dipole interaction strengths, respectively. The transverse pump profile is assumed to be wide enough to take h_0 uniform. Dipole approximation is used for the transverse direction. After adiabatically eliminating ψ_e, under the condition of $\Delta_0 = \omega_0 - \omega_{be}$ being larger than the excited state linewidth, the Hamiltonian reduces to

$$H = \sum_{j=b,c} \int \mathrm{d}x\ \psi_j^\dagger \mathcal{H} \psi_j + \sum_{i,j=b,c} \int \mathrm{d}x\ \frac{u_{ij}}{2}\psi_i^\dagger \psi_j^\dagger \psi_j \psi_i - \hbar\delta_c a^\dagger a - \mathrm{i}\hbar\eta_{||}(a - a^\dagger), \quad (3)$$

where, in a rotating frame defined by the unitary operator $U = \exp(-\mathrm{i}\omega_0 t a^\dagger a)$,

$$\mathcal{H} = -\frac{\hbar^2}{2m}\frac{\partial^2}{\partial x^2} + \left(\frac{2\hbar h_0^2}{\Delta_0} + V_b(x) \right) \sigma^- \sigma^+ + \left(\hbar U_0 \cos^2(kx)(aa^\dagger + a^\dagger a) + V_c(x) + \hbar\omega_{bc} \right) \sigma^+ \sigma^- + \hbar\eta(a + a^\dagger)\cos(kx)(\sigma^- + \sigma^+). \quad (4)$$

Here $U_0 = g_0^2/\Delta_0$, $\eta = h_0 g_0/\Delta_0$, $\delta_c = \omega_0 - \omega_c$ [9], $\sigma^+ = |c\rangle\langle b|$ and $\sigma^- = |b\rangle\langle c|$.

The early stages of the dynamics are strongly influenced by quantum fluctuations that trigger the superradiance. We consider the late time dynamics in which the condensate and field variables are assumed to be classical [33]. The effect of quantum fluctuations is introduced by seeding the cavity field in numerical simulations. In our case seeding is performed either by adding very small fluctuations proportional to $\cos(kx)$ to ψ_c (cf section 3) when there is no parallel pump, or physically by the parallel pump that drives the cavity (cf section 4).

The Heisenberg equations of motion in this mean-field regime take the following form:

$$\dot{\psi}_b = -\frac{\mathrm{i}}{\hbar}\left(-\frac{\hbar^2}{2m}\frac{\partial^2}{\partial x^2} + V_b(x) + \frac{2\hbar h_0^2}{\Delta_0} + u_{bb}|\psi_b|^2 + u_{bc}|\psi_c|^2\right)\psi_b - \frac{\mathrm{i}}{\hbar}V_1\psi_c, \tag{5}$$

$$\dot{\psi}_c = -\frac{\mathrm{i}}{\hbar}\left(-\frac{\hbar^2}{2m}\frac{\partial^2}{\partial x^2} + V_c(x) + \hbar\omega_{bc} + V_2 + u_{cc}|\psi_c|^2 + u_{bc}|\psi_b|^2\right)\psi_c - \frac{\mathrm{i}}{\hbar}V_1\psi_b, \tag{6}$$

$$\dot{\alpha} = \mathrm{i}\left(\mathrm{i}\kappa + \delta_c - 2U_0\int \mathrm{d}x\ |\psi_c|^2\cos^2(kx)\right)\alpha - \mathrm{i}\eta\int \mathrm{d}x\ \cos(kx)(\psi_c^*\psi_b + \psi_b^*\psi_c) + \eta_{||}, \tag{7}$$

where α_r is the real part of the cavity field α and κ is the phenomenological decay rate of the cavity [33]. Here $V_1 = 2\hbar\eta\cos(kx)\alpha_\mathrm{r}$ is the spatially modulated rate of the Raman transition. $V_2 = 2\hbar U_0\cos^2(kx)|\alpha|^2$ is a standing wave trapping potential for atoms in state $|c\rangle$ which has been built by the cavity mode. The minima of V_2 trap the atoms in $|c\rangle$ at $x_j = j\lambda/2$, where j is an integer and λ is the wavelength of the cavity mode. In return, atoms in state $|c\rangle$ cause a shift in the cavity resonance due to their spatial overlap with the cavity mode by $-2U_0\int \mathrm{d}x\ |\psi_c|^2\cos^2(kx)$.

Up to this point we have included the effect of an extra parallel pump in the dynamics of the system. However, in section 3 we study the phase transition without this parallel laser pump and later in section 4, where we consider practical ways of synthesizing a sharper and robust lattice, we will address its effect.

3. Phase transition and formation of a spin lattice

In an optical cavity, superradiance is identified by an abrupt increase in the number of cavity photons $n = |\alpha|^2$ and Raman transition is monitored with the total magnetization $Z = \int \mathrm{d}x\ Z(x,t)$, where $Z(x,t) = (|\psi_b(x,t)|^2 - |\psi_c(x,t)|^2)/N$ is the magnetization density that is normalized by the total number of atoms $N = \int \mathrm{d}x(|\psi_b(x,t)|^2 + |\psi_c(x,t)|^2)$. The total magnetization can have extremum values 1 and -1 when all atoms are in mode $|b\rangle$ or $|c\rangle$, respectively. Therefore, if initially all atoms are in hyperfine state $|b\rangle$, the Raman superradiance is identified by a sudden increase in the number of cavity photons accompanied by an abrupt decrease in the value of total magnetization Z.

The Dicke phase transition, in single-mode condensates, takes place between two different momentum states of the condensate atoms which leads to density grating and is identified by an order parameter which measures the overlap of density distribution and cavity mode profile. In our system though, we will show that the density grating happens only for the atoms in hyperfine state $|c\rangle$ and therefore a polarization (magnetization) grating will occur. This translational symmetry breaking in magnetization density $Z(x,t)$ is also identified by an order parameter, which we will introduce later in section 3.1.

Since the potential V_1 defines the rate of Raman scattering and transition of atoms between the two hyperfine states, the atoms on the antinodes of $\cos(kx)$ are highly affected by Raman scattering (figure 2) while those that are on the nodes are protected. On the other hand if we choose Δ_0 (and consequently U_0) to be negative, then the minima of the trapping potential V_2 will coincide with the antinodes of V_1. In this way, overlap of different hyperfine spin states, which act as an atomic polarization grating, is enhanced around the antinodes and stimulates even more Raman scattering, which completes a self-consistency loop for a self-organization

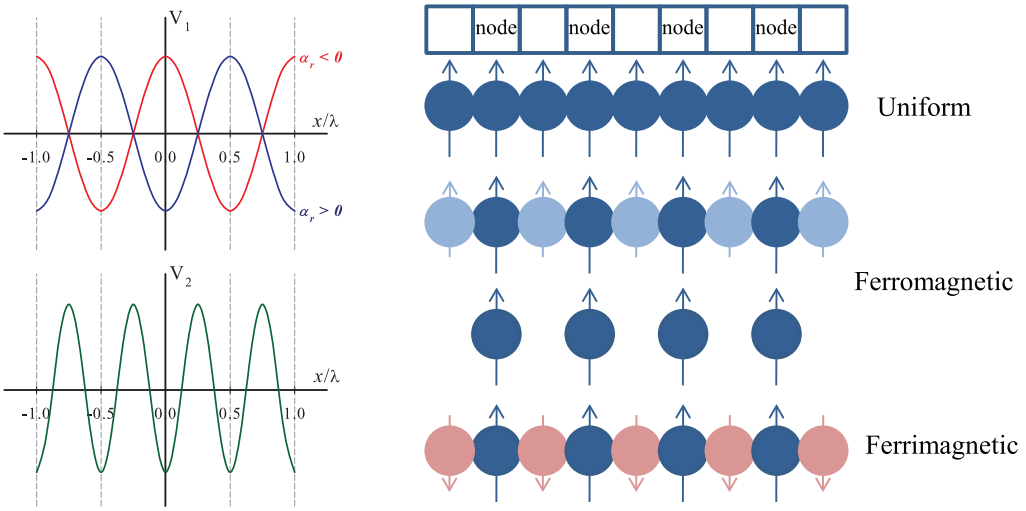

Figure 2. Left: schematic drawing of potentials V_1 and V_2 as functions of x when Δ_0, and consequently U_0 and η are chosen to be negative. x is scaled by the wavelength of the cavity mode λ. V_1 defines the rate of Raman transition and V_2 is a trapping potential for atoms in the hyperfine state $|c\rangle$. Right: while the atoms on the nodes of $\cos(kx)$ are protected from Raman scattering, depending on the rate of transition V_1 on the antinodes, formation of ferromagnetic or ferrimagnetic lattices is possible. Blue circles with upward arrows represent positive magnetization and red circles with downward arrows show negative magnetization. Lighter (darker) colors and shorter (longer) arrows represent smaller (larger) magnetization.

process. Accumulation of the atoms in $|c\rangle$ around the antinodes and protection of atoms in $|b\rangle$ from Raman scattering around the nodes of the cavity mode result in a spatial distillation of magnetization, manifested as a self-organized magnetic lattice with a lattice constant $\lambda/2$. In other words, the magnetization on the nodes of the cavity mode will always be positive, while, depending on the rate of Raman transition, antinodes can have positive, zero or negative magnetization (figure 2) and therefore synthesis of a ferromagnetic or ferrimagnetic lattice would be possible.

On the right side of figure 2, the first row from top, with dark blue circles, represents the uniform condensate of atoms all in state $|b\rangle$ which is the initial setup of the system. Assuming that all atoms are initially in state $|b\rangle$ practically means that the condensate is kept at such a low temperature that transition to higher state $|c\rangle$ due to inelastic atomic collisions is energetically forbidden. As an example, the ^{87}Rb condensate can have a typical temperature of the order of 200 nK or less [42, 45]. Therefore, in such a condensate, transition between hyperfine states due to inelastic atomic collisions is highly suppressed if those states are energetically apart by 13 kHz or more. The second row in figure 2 shows the case where less than half of the atoms on the antinodes are Raman scattered from $|b\rangle$ to $|c\rangle$, giving rise to a smaller, but still positive, value of magnetization. If 50% or more of the atoms are scattered from $|b\rangle$ to $|c\rangle$, then magnetization on the antinodes would become zero (third row) or negative (last row), resulting in the formation of ferromagnetic or ferrimagnetic lattices.

3.1. Critical value of pump strength for the phase transition

In order to analytically calculate the critical strength of transverse pump η_c, for which the system undergoes superradiance and self-organization, we first study the steady-state properties of the system. We assume that in the steady state $\dot{\alpha} = 0$ and therefore, by introducing $\theta = \int \mathrm{d}x\ \psi_c^*(x,t)\cos(kx)\psi_b(x,t)$, $\beta = \int \mathrm{d}x\ \psi_c^*(x,t)\cos^2(kx)\psi_c(x,t)$ and $\bar{\delta_c} = \delta_c - 2U_0\beta$, the steady cavity field can be expressed as

$$\alpha = \frac{2\theta_\mathrm{r}\eta}{\mathrm{i}\kappa + \bar{\delta_c}} \tag{8}$$

with θ_r being the real part of θ. As mentioned earlier, $-2U_0\beta$ is the shift in the cavity mode frequency caused by atoms in state $|c\rangle$ while β measures the bunching of atoms in state $|c\rangle$ inside the minima of the trapping potential V_2. The parameter θ shows the overlap of the cavity mode function $\cos(kx)$ with the spin polarization grating and can be considered as an order parameter for self-organization of magnetization. We emphasize that, in contrast to the case of single-component BEC in an optical cavity [5], V_1 here is the Raman transition rate and not a trapping potential. In a single-component BEC system, different signs of the order parameter lead to two different lattice structures after translational symmetry breaking, when atoms are localized around the even ($kx = 2n\pi$) or odd ($kx = (2n+1)\pi$) antinodes of the field. In our system, breaking of the Z_2 symmetry also happens but it is not manifested by the appearance of different lattice structures. Both even and odd antinode locations are sites for Raman interactions that lead to the same lattice but with different magnetic character depending on the strength of the Raman coupling. Therefore, different signs of θ_r or α_r do not correspond to different (even and odd) lattice structures and a nonzero value of order parameter θ is sufficient to indicate the phase transition.

Regarding the wavefunctions of the condensate, in steady state, we assume that they can be written in the form $\psi_b(x,t) = \psi_b(x)\exp(-\mathrm{i}\mu_b t/\hbar)$ and $\psi_c(x,t) = \psi_c(x)\exp(-\mathrm{i}\mu_c t/\hbar)$, with μ being the chemical potential; then the dynamical equations (5) and (6) in the absence of external trap potentials will become

$$\mu_b\psi_b(x) = \left(-\frac{\hbar^2}{2m}\frac{\partial^2}{\partial x^2} + \frac{2\hbar h_0^2}{\Delta_0} + u_{bb}|\psi_b|^2 + u_{bc}|\psi_c|^2\right)\psi_b(x) + V_1\psi_c(x)\mathrm{e}^{-\frac{\mathrm{i}}{\hbar}\Delta\mu t}, \tag{9}$$

$$\mu_c\psi_c(x) = \left(-\frac{\hbar^2}{2m}\frac{\partial^2}{\partial x^2} + \hbar\omega_{bc} + V_2 + u_{cc}|\psi_c|^2 + u_{bc}|\psi_b|^2\right)\psi_c(x) + V_1\psi_b(x)\mathrm{e}^{\frac{\mathrm{i}}{\hbar}\Delta\mu t}, \tag{10}$$

where $\Delta\mu = \mu_c - \mu_b$.

For a system in which all atoms are initially in state $|b\rangle$ and are homogeneously distributed, the initial wavefunctions are $\psi_b(x) = \sqrt{N/L}$ and $\psi_c(x) = 0$. Substituting these initial conditions into (8)–(10) results in $\alpha = 0$, $\mu_b = 2\hbar h_0^2/\Delta_0 + u_{bb}N/L$ and $2\sqrt{N/L}\alpha_\mathrm{r}\eta\cos(kx)\exp(\mathrm{i}\Delta\mu t/\hbar) = 0$. The latter is satisfied because with the choice of initial conditions, θ and consequently α are zero, and this means that $\psi_c = 0$ is a stable solution of equations of motion as long as the cavity field is zero. Therefore to destabilize ψ_c, one needs to have a nonzero cavity field that, in the simplest case, can be achieved by adding a perturbation term with $\cos(kx)$ modulation to the stable $\psi_c(x,0)$. Therefore, the perturbed system will be defined with $\psi_b(x,t) = \sqrt{N/L}$, $\psi_c(x,t) = \sqrt{N/L}\epsilon\cos(kx)$ and $\alpha = N\epsilon\eta/(\mathrm{i}\kappa + \delta_c)$. If this fluctuation in ψ_c survives and grows, as a consequence, the order parameter θ and cavity field α will grow as well. A larger cavity field, in return, will advance the rate of Raman

transition and will deepen the trapping potential for atoms in $|c\rangle$. These will lead to an even larger order parameter and, as a result of this positive feedback loop, superradiance and phase transition, which are characterized by an abrupt change in cavity photon number and magnetization, will take place. To calculate the critical value of pump strength for which the transition occurs, we evolve the system one step of imaginary time, starting from the perturbed state:

$$\frac{\Delta\psi_b}{\Delta\tau} = -\left(\frac{2\eta^2}{U_0} + \frac{Nu_{bb}}{\hbar L}\right)\sqrt{N/L}, \tag{11}$$

$$\frac{\Delta\psi_c}{\Delta\tau} = -\left(\omega_{\rm r} + \omega_{bc} + \frac{Nu_{bc}}{\hbar L} + \frac{2N\eta^2\delta_c}{\kappa^2+\delta_c^2}\right)\sqrt{N/L}\epsilon\cos(kx), \tag{12}$$

where $\tau = {\rm i}\,t$ is the imaginary time and we have used $h_0^2/\Delta_0 = \eta^2/U_0$ in the first term on the right-hand side of (11) in order to show the η-dependence of decay rates more clearly.

According to (11), $\psi_b(x,t)$ exhibits an expected decay with a rate equal to $\mu_b/\hbar = 2h_0^2/\Delta_0 + Nu_{bb}/(\hbar L)$. However, the situation for $\psi_c(x,t)$ depends on the sign of the perturbation term decay rate (terms inside the parentheses in (12)). With the positive cavity–pump detuning δ_c, this decay rate is always positive and perturbation will not survive. However if δ_c is negative, then this decay rate would be negative as well if

$$N\eta^2 > \left(\omega_{\rm r} + \omega_{bc} + \frac{Nu_{bc}}{\hbar L}\right)\frac{(\kappa^2+\delta_c^2)}{2|\delta_c|} \tag{13}$$

and therefore we find for critical transverse pump strength $\eta_{\rm c}$

$$\sqrt{N}|\eta_{\rm c}| = \sqrt{\left(\omega_{\rm r} + \omega_{bc} + \frac{Nu_{bc}}{\hbar L}\right)\frac{(\kappa^2+\delta_c^2)}{2|\delta_c|}}. \tag{14}$$

One should notice that $\eta_{\rm c}$ in (14) does not depend on U_0 because in our system, the effective trapping potential V_2 is created only for atoms in mode $|c\rangle$ and therefore, in return, the phase shift of the cavity mode resonance depends on the number of atoms in mode $|c\rangle$ which is initially negligible within the first-order perturbation. For $\omega_{bc} = \omega_{\rm r}$, $N = 48\times10^3$, $L = 2\,\lambda$, $\kappa = 400\,\omega_{\rm r}$ and $\delta_c = -4800\,\omega_{\rm r}$ [22], we find $|\eta_c| \approx 2.16\,\omega_{\rm r}$ if the atom–atom interaction strength $u_{bc} \approx 3.8\times10^{-3}\,\lambda\omega_{\rm r}$.

3.2. Numerical results

In this section, the results of the numerical solution of the dynamical equations (5)–(7) will be presented. Using the second-order split step method, and assuming all atoms are initially in the hyperfine spin state $|b\rangle$, the mean-field equations are solved numerically to monitor the dynamics of the system.

Figure 3 demonstrates the dynamics of the cavity photon number n, total magnetization Z, the order parameter $\theta_{\rm r}$ (all on the left panels) as well as the spatio-temporal behavior of magnetization density $Z(x,t)$ (on the right) when the transverse pump has the strength $\eta = -3\,\omega_{\rm r}$. We have considered a cavity with wavelength $\lambda = 800\,$nm [22] which for rubidium atoms gives a recoil frequency of $\omega_{\rm r} \sim 20\,$kHz. Other parameters used for this

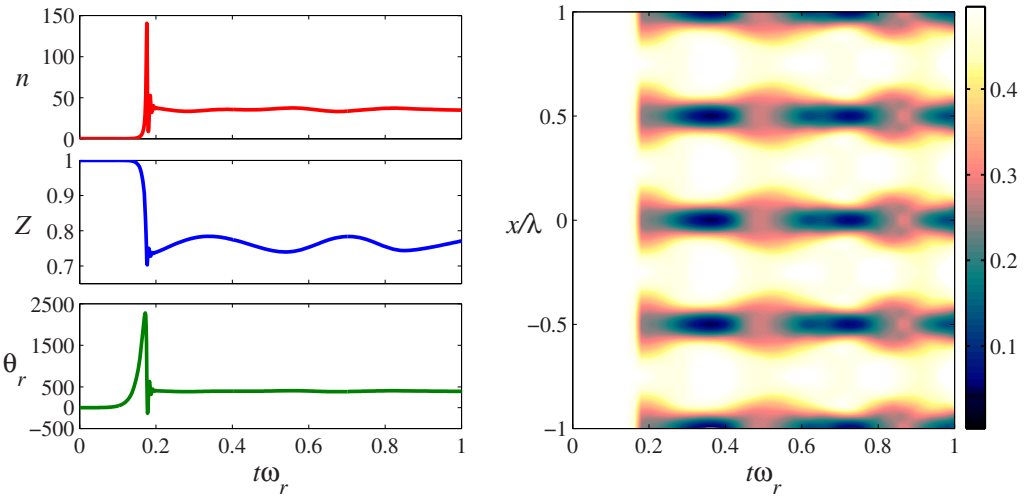

Figure 3. Left: dynamics of the cavity photon number n, total magnetization Z and the real part of order parameter $\theta_{\rm r}$. Right: spatial and dynamical behavior of magnetization density $Z(x,t)$ of the same system. Here, the system is subject to a transverse pump with fixed strength $\eta = -3\ \omega_{\rm r}$ and other parameters, in units of $\omega_{\rm r}$, are $\omega_{bc} = 1$, $\kappa = 400$, $U_0 = -0.5$, $\delta_c = -4800$, $\Delta_0 = -4 \times 10^6$ and $N = 48 \times 10^3$.

simulation, in units of $\omega_{\rm r}$, are $\omega_{bc} = 1$, $\kappa = 400$, $\delta_c = -4800$ [22], $U_0 = -0.5$ and $\Delta_0 = -4 \times 10^6$. We have considered a condensate of $N = 48 \times 10^3$, atom–atom interaction strengths $u_{bc} = u_{cb} \approx 3.8 \times 10^{-3}\,\lambda\omega_{\rm r}$ and $u_{bb} = u_{cc} \approx 4.5 \times 10^{-3}\,\lambda\omega_{\rm r}$. One can see in figure 3 that superradiance and phase transition take place at $t \sim 0.2\,\omega_{\rm r}$ after the system is pumped with the transverse laser with strength $\eta = -3\,\omega_{\rm r}$. While cavity photon number, total magnetization and order parameter reach slowly oscillating steady states, a ferromagnetic lattice of magnetization is formed. Since atoms initially were in state $|b\rangle$, total magnetization Z is equal to one before the phase transition. On the other hand, atoms are initially distributed in an area with length $L = 2\,\lambda$ homogeneously which gives rise to magnetization $Z(x,t) = 0.5$ throughout the condensate. In this case after the transition less than (but very close to) 50% of atoms on the antinodes of the potential V_1 are scattered to state $|c\rangle$, causing a very small positive value of magnetization around the antinodes. However, the atoms on the nodes are almost untouched as expected.

Since the scattering rate V_1 and cavity field α are proportional to the transverse pump strength η, one would expect a higher percentage of atoms around the antinodes of V_1 being scattered to $|c\rangle$ by simply using a larger η. Figure 4 shows the dynamics of the system with $\eta = -8\,\omega_{\rm r}$ where a ferrimagnetic lattice of magnetization is created due to transition of more than 50% of atoms on antinodes from state $|b\rangle$ to $|c\rangle$. Apart from η, all the other parameters are similar to those used in figure 3, and the spatio-temporal behavior of magnetization $Z(x,t)$ is shown for a longer time in order to present a clearer view of the spin lattice.

Although the perturbation method in section 3.1 predicts a phase transition for the transverse pump with strength $2.16\,\omega_{\rm r}$ or above, numerical solution leads to a phase transition with values of pump strength smaller than the value predicted by the perturbation method. In the numerical method, no phase transition occurs with $\eta \leqslant 1.85\,\omega_{\rm r}$.

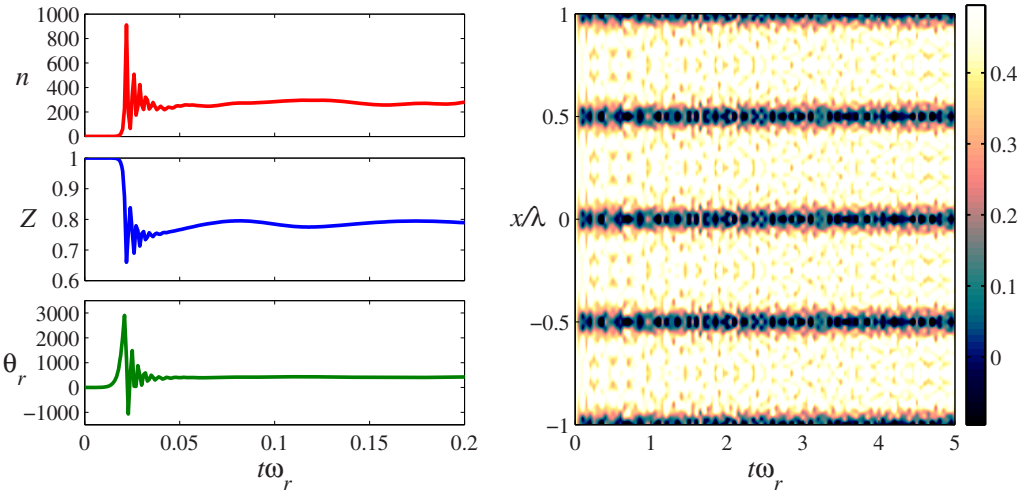

Figure 4. Left: dynamics of the cavity photon number n, total magnetization Z and the real part of order parameter θ_{r}. Left: spatial and dynamical behavior of magnetization density $Z(x, t)$ of the same system is shown in a wider range of time to give a better view of the synthesized lattice. In this case, the system is subject to a transverse pump with fixed strength $\eta = -8\,\omega_{\mathrm{r}}$ and the other parameters are the same as those in figure 3.

4. Practical synthesis of a robust spin lattice

In this section, we address some practical issues that might be helpful in the implementation of a sharp and robust spin lattice. First of all, we recall that in the last section the strength of the transverse pump was assumed to be constant. However, considering a time-dependent pump is more practical. In the experiments, the power of the pump is usually ramped up in time so that it is initially zero and increases gradually. In numerics, using a ramped-up pump delays the time of transition because during the early stages the system is subject to a laser with smaller values of strength. This would give more control on the system at the time of transition. Moreover, one would think of having a robust lattice without the need of an all-time-on laser field. In other words, it would be desirable to turn off the laser pump after synthesis of the spin lattice. We will show numerically that it is possible to have a robust lattice even when the laser pump is switched off after the transition. The fact that the atoms on the nodes of V_1 remain untouched and therefore around the nodes there exists a single-component condensate while around the antinodes both modes are occupied is the reason for this robustness. When the pump is switched off ($\eta = 0$), the Raman coupling terms (last terms) in (5) and (6) vanish and these equations are reduced to equations of motion of a two-component condensate with atom–atom interaction. Due to the difference between the chemical potentials of the two components, there will be coherent oscillations in their wavefunctions [46, 47] and consequently in the magnetization. This is the case around the antinodes while, around the nodes, the single-component condensate remains stable.

Another point to be considered is the role of an extra laser pump, parallel to the cavity axis. A parallel laser pump can contribute to the cavity field as shown in (7) so that the steady cavity

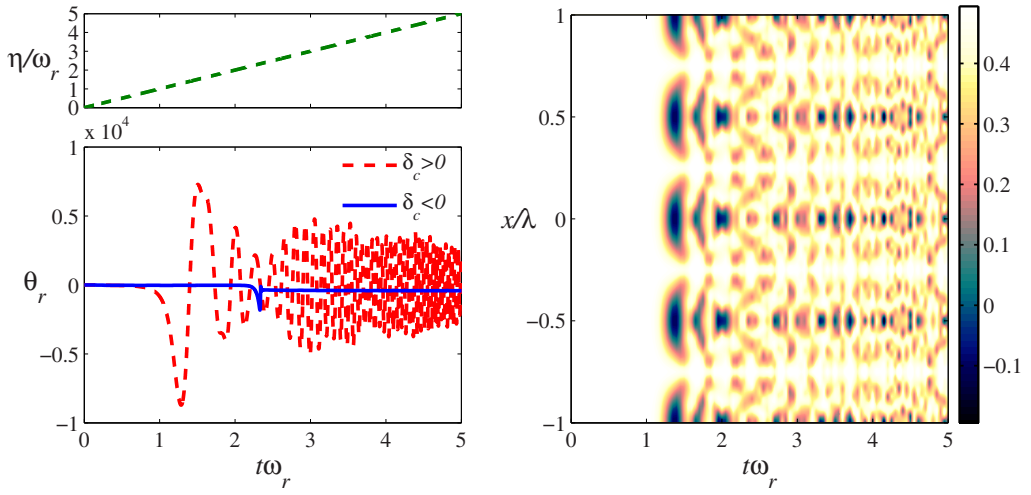

Figure 5. Left: time dependence of the strength of an effective transverse laser pump η and dynamics of the real part of order parameter $\theta_{\rm r}$, with fixed parallel pump strength $\eta_{\parallel} = 1000\,\omega_{\rm r}$ and for positive and negative cavity–pump detuning δ_c. Right: spatial and dynamical behavior of magnetization density $Z(x,t)$ for the case of positive δ_c which shows synthesis of a sharp lattice around time $t \approx 1.4/\omega_{\rm r}$ when $\eta \approx 1.4\,\omega_{\rm r}$. Here, in units of $\omega_{\rm r}$, $\omega_{bc} = 1$, $\kappa = 400$, $U_0 = -0.5$, $|\delta_c| = 4800$, $\Delta_0 = -4 \times 10^6$ and $N = 48 \times 10^3$.

field takes the following form:

$$\alpha = \frac{2\theta_{\rm r}\eta + {\rm i}\eta_{\parallel}}{{\rm i}\kappa + \bar{\delta}_c}. \tag{15}$$

In addition to seeding the cavity field instead of relying on fluctuations to trigger the phase transition, a strong parallel pump can also affect the depth of the trapping potential V_2 as well as the rate of scattering V_1 indirectly through the cavity field. These latter facts would allow the formation of a sharper spin lattice with smaller values of transverse pump strength. More interestingly, through its effect on V_2 and consequently the decay rate of fluctuations in ψ_c, a parallel pump can open up the possibility of formation of a spin lattice with both positive and negative cavity–pump detuning δ_c.

To bring all the above points together, in figure 5 we show the real part of order parameter $\theta_{\rm r}$ as a function of time for the two cases with positive and negative cavity–pump detuning δ_c, while parallel pump strength is fixed to $\eta_{\parallel} = 1000\,\omega_{\rm r}$ and transverse pump strength is ramped up from zero at $t = 0$ to $\eta = -5\,\omega_{\rm r}$ at time $t = 5/\omega_{\rm r}$. In the case with positive δ_c, cavity photon number n and magnetization Z exhibit oscillatory behavior similar to $\theta_{\rm r}$ after the transition. For the case with negative δ_c, Z saturates to a stationary value while n increases due to the increase in the pump strength.

In both cases, with positive or negative δ_c, the order parameter is initially zero as a sign of a homogeneous condensate. Then, when a critical value of transverse pump strength η is reached, Raman superradiance takes place and simultaneously a polarization grating happens due to accumulation of atoms in state $|c\rangle$ on the antinodes of the cavity mode function. As a consequence of the translational symmetry breaking, the value of $\theta_{\rm r}$ becomes nonzero. Since any change in the value of the order parameter is a sign of the change in the value or distribution

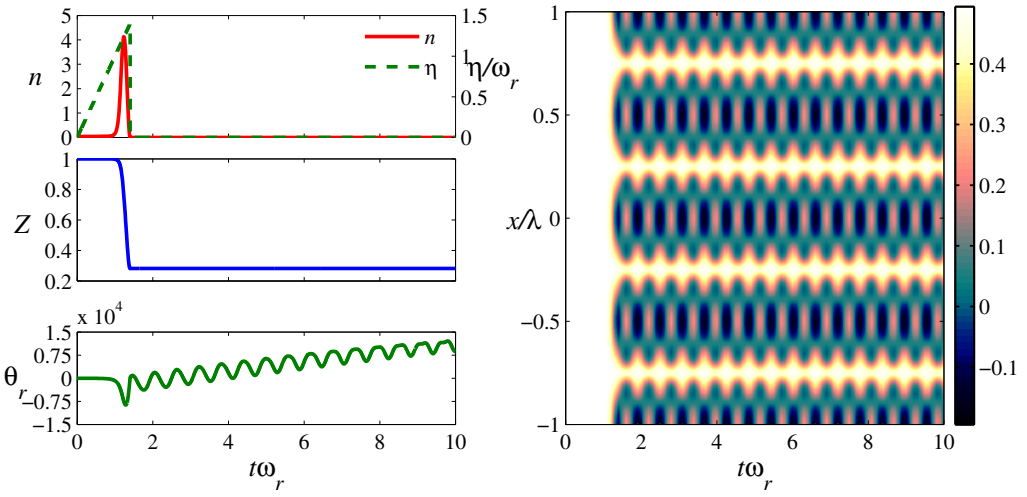

Figure 6. Left: time dependence of the strength of an effective transverse laser pump η (dashed line) and dynamics of the cavity photon number n, total magnetization Z and real part of order parameter $\theta_{\rm r}$. Right: spatial and dynamical behavior of magnetization density $Z(x,t)$. In this case, parallel pump strength has been fixed to $\eta_{\parallel} = 1000\,\omega_{\rm r}$ while transverse pump strength has been ramped up from zero at $t = 0$ to $\eta = -1.4\,\omega_{\rm r}$ at $t = 1.4/\omega_{\rm r}$, and then both pumps are turned off when the spin lattice has taken a well-defined shape. Other parameters are the same as those in figure 5 with positive δ_c.

of magnetization around the antinodes of the cavity mode, by looking at the oscillations of $\theta_{\rm r}$ in figure 5 for positive δ_c, one would expect oscillations in the magnetization density around the antinodes for this case. In the right panel of figure 5, the spatio-temporal behavior of magnetization density $Z(x,t)$ of the case with positive δ_c is also shown, which demonstrates the expected oscillations. The case with negative δ_c exhibits a stable lattice structure; however, the lattice is never as well-defined as the one with positive δ_c at $t \sim 1.4/\omega_{\rm r}$. The value of the order parameter in the left side of figure 5 is a clear sign of this fact.

Although magnetization density of the case with positive δ_c oscillates in time, it clearly demonstrates synthesis of a very sharp lattice around $t \sim 1.4/\omega_{\rm r}$ when $\eta \sim -1.4\ \omega_{\rm r}$. From the right panel of figure 5 one can observe that, as the pump is ramped up, the magnetized domains are not well isolated from the de-magnetized ones and there is no robust spin lattice structure for this case. This problem can be avoided by turning both laser pumps off when the lattice has taken the desired shape. Figure 6 shows the dynamics of cavity photon number n, total magnetization Z, order parameter $\theta_{\rm r}$, as well as magnetization density $Z(x,t)$ for the case with positive δ_c and fixed parallel pump $\eta_{\parallel} = 1000\ \omega_{\rm r}$, when both pumps are abruptly turned off at time $t = 1.4/\omega_{\rm r}$. At this point, due to the lack of Raman transition, magnetization Z remains a constant and all the photons leave the cavity. In the absence of the laser pumps, the regions around the antinodes of the cavity mode exhibit oscillatory behavior as expected. However, nodes with maximum positive magnetization remain untouched and are very well separated from each other. Since there is no laser pumping the system, one would not expect a net change in the order parameter. In fact, the increase in $\theta_{\rm r}$, observed in figure 6, is a part of a very slow oscillatory behavior. In other words, $\theta_{\rm r}$ exhibits some fast oscillations as well as slow oscillations.

5. Conclusion

We conclude that a BEC with two non-degenerate hyperfine spin components in a high-finesse cavity driven by a transverse pump can exhibit Raman superradiance above a critical value of the transverse field strength. Simultaneously, the BEC undergoes a phase transition, associated with both the external and internal degrees of freedom, during which atoms scatter a transverse laser field into the cavity mode and in return their hyperfine state changes. As a result, the cavity photon number rises abruptly and at the same time there is a sudden increase in the population of the higher hyperfine state at periodic positions exhibiting a magnetic lattice configuration. An extra laser pump parallel to the cavity axis can be used in order to synthesize sharper lattices and the lattice remains robust after turning both laser pumps off. Even though the present analysis is in the mean-field regime, we can envision that hyperfine spins at different lattice sites would be entangled as they interact with the common cavity field, following the resonant entanglement of atoms in the multitraps scenario [48]. The availability of a large number of spins per site could make the system advantageous for exploring magnetic supersolid properties. In contrast to Rayleigh superradiance, Raman superradiance can be used as a source of entangled photon-spin pairs. The application of cold atoms in optical lattices for quantum information purposes has been a developing field of theoretical and experimental studies [49–51]. In addition to optical lattices, spin systems are commonly considered for quantum information bits (qubits) and associated quantum information processing. Our treatment brings optical lattices and spin lattices together in a compact and controllable cavity-QED environment. Synthesis and probing robust spin lattice models with fast superradiance-induced phase transition and self-organization properties promise unique opportunities for quantum information applications as well as monitoring phase transitions and spin correlations with the Raman scheme. Long-range spin–spin interactions induced by the cavity field can be utilized on an optical spin lattice created in the cavity. Large spin values at the sites together with the coherence from the underlying condensate can be useful for quantum memory as well as information processing. Moreover, leaking photons from the cavity and external drives can be used for non-destructive probing and accessing the system. We hope our work will stimulate further research in this direction.

Acknowledgments

This work was supported by TÜBİTAK (grant numbers 109T267, 112T176 and 112T974), TUBA and Bilkent University.

References

[1] Mekhov I B and Ritsch H 2012 *J. Phys. B: At. Mol. Opt. Phys.* **45** 102001
[2] Ritsch H, Domokos P, Brennecke F and Esslinger T 2013 *Rev. Mod. Phys.* **85** 553
[3] Domokos P and Ritsch H 2002 *Phys. Rev. Lett.* **89** 253003
[4] Black A T, Chan H W and Vuletić V 2003 *Phys. Rev. Lett.* **91** 203001
[5] Nagy D, Szirmai G and Domokos P 2008 *Eur. Phys. J.* D **48** 127
[6] Kónya G, Szirmai G and Domokos P 2011 *Eur. Phys. J.* D **65** 33
[7] Bux S, Gnahm C, Maier R A W, Zimmermann C and Courteille P W 2011 *Phys. Rev. Lett.* **106** 203601
[8] Horak P, Barnett S M and Ritsch H 2000 *Phys. Rev.* A **61** 033609
[9] Brennecke F, Donner T, Ritter S, Bourdel T, Köhl M and Esslinger T 2007 *Nature* **450** 268

[10] Colombe Y, Steinmetz T, Dubois G, Linke F, Hunger D and Reichel J 2007 *Nature* **450** 272
[11] Slama S, Bux S, Krenz G, Zimmermann C and Courteille P W 2007 *Phys. Rev. Lett.* **98** 053603
[12] Wolke M, Klinner J, Keßler H and Hemmerich A 2012 *Science* **337** 75
[13] Elsässer T, Nagorny B and Hemmerich A 2004 *Phys. Rev.* A **69** 033403
[14] Gupta S, Moore K L, Murch K W and Stamper-Kurn D M 2007 *Phys. Rev. Lett.* **99** 213601
[15] Ritter S, Brennecke F, Baumann K, Donner T, Guerlin C and Esslinger T 2009 *Appl. Phys.* B **95** 213
[16] Safaei S, Müstecaplıoğlu Ö E and Tanatar B 2013 *Laser Phys.* **23** 035501
[17] Mekhov I B, Maschler C and Ritsch H 2007 *Nature Phys.* **3** 319
[18] Dicke R H 1954 *Phys. Rev.* **93** 99
[19] Hepp K and Lieb E H 1973 *Ann. Phys.* **76** 360
[20] Wang Y K and Hioe F T 1973 *Phys. Rev.* A **7** 831
[21] Nagy D, Kónya G, Szirmai G and Domokos P 2010 *Phys. Rev. Lett.* **104** 130401
[22] Baumann K, Guerlin C, Brennecke F and Esslinger T 2010 *Nature* **464** 1301
[23] Baumann K, Mottl R, Brennecke F and Esslinger T 2011 *Phys. Rev. Lett.* **107** 140402
[24] Bhaseen M J, Mayoh J, Simons B D and Keeling J 2012 *Phys. Rev.* A **85** 013817
[25] Dalla Torre E G, Diehl S, Lukin M D, Sachdev S and Strack P 2013 *Phys. Rev.* A **87** 023831
[26] Kónya G, Nagy D, Szirmai G and Domokos P 2012 *Phys. Rev.* A **86** 013641
[27] Öztop B, Bordyuh M, Müstecaplıoğlu Ö E and Türeci H E 2012 *New J. Phys.* **14** 085011
[28] Nagy D, Szirmai G and Domokos P 2011 *Phys. Rev.* A **84** 043637
[29] Yukalov V I 2009 *Laser Phys.* **19** 1
[30] Schneble D, Campbell G K, Streed E W, Boyd M, Pritchard D E and Ketterle W 2004 *Phys. Rev.* A **69** 041601
[31] Yoshikawa Y, Sugiura T, Torii Y and Kuga T 2004 *Phys. Rev.* A **69** 041603
[32] Cola M M and Piovella N 2004 *Phys. Rev.* A **70** 045601
[33] Uys H and Meystre P 2007 *Phys. Rev.* A **75** 033805
[34] Huang J-S, Xie Z-W and Wei L-F 2011 *Commun. Theor. Phys.* **55** 59
[35] Strack P and Sachdev S 2011 *Phys. Rev. Lett.* **107** 277202
[36] Zhou L, Pu H, Ling H Y and Zhang W 2009 *Phys. Rev. Lett.* **103** 160403
[37] Zhou L, Pu H, Ling H Y, Zhang K and Zhang W 2010 *Phys. Rev.* A **81** 063641
[38] Dong Y, Ye J and Pu H 2011 *Phys. Rev.* A **83** 031608
[39] Grießer T, Niedenzu W and Ritsch H 2012 *New J. Phys.* **14** 053031
[40] Guo L, Chen S, Frigan B, You L and Zhang Y 2009 *Phys. Rev.* A **79** 013630
[41] Kagan Yu, Svistunov B V and Shlyapnikov G V 1985 *JETP Lett.* **42** 209
[42] Burt E A, Ghrist R W, Myatt C J, Holland M J, Cornell E A and Wieman C E 1997 *Phys. Rev. Lett.* **79** 337
[43] Ketterle W and Miesner H J 1997 *Phys. Rev.* A **56** 3291
[44] Gangl M and Ritsch H 2002 *J. Phys. B: At. Mol. Opt. Phys.* **35** 4565
[45] Anderson M H, Ensher J R, Matthews M R, Wieman C E and Cornell E A 1995 *Science* **269** 198
[46] Busch T and Anglin J R 2001 *Phys. Rev. Lett.* **87** 010401
[47] Das P, Raju T S, Roy U and Panigrahi P K 2009 *Phys. Rev.* A **79** 015601
[48] Yukalov V I and Yukalova E P 2006 *Phys. Rev.* A **73** 022335
[49] Braunstein S L and Lo H-K 2001 *Scalable Quantum Computers: Paving the Way to Realization* (Berlin: Wiley-VCH)
[50] Jaksch D and Zoller P 2005 *Ann. Phys.* **315** 52
[51] Treutlein P *et al* 2006 *Fortschr. Phys.* **54** 702